Journal of Molecular Modeling (2020) 26: 91
https://doi.org/10.1007/s00894-020-04357-w

ORIGINAL PAPER

# Theoretical study on the activation of C-H bond in ethane by $PdX^+$ (X = F, Cl, Br, H, and $CH_3$) in the gas phase

Yu-Xiu Nie[1] · Xiao-Xia Zhang[1] · Yong-Ning Yuan[1] · Feng Lu[1] · Zhi-Yuan Geng[1]

Received: 16 January 2020 / Accepted: 18 March 2020 / Published online: 3 April 2020


## Abstract

The mechanism of C-H bond activation of ethane was catalyzed by palladium halide cations ($PdX^+$ (X = F, Cl, Br, H, and $CH_3$)), which was investigated using density functional theory (DFT) at B3LYP level. The reaction mechanism was taken into account in triplet and singlet spin state potential energy surfaces. For $PdF^+$, $PdCl^+$, and $PdBr^+$, the high spin states were the ground states, whereas the ground states were the low spin states in $PdH^+$ and $PdCH_3^+$. The reaction of $PdF^+$, $PdCl^+$, and $PdBr^+$ with ethane occurred via a typical "two-state reactivity" mechanism. In contrast, for $PdH^+$ and $PdCH_3^+$, the overall reaction performed on the ground state PESs in a spin-conserving manner. The crossing points between two potential energy surfaces were observed and effectively decreased the activation barrier in $PdX^+/C_2H_6$ (X = F, Cl, and Br). The minimum energy crossing points (MECP) were obtained used the algorithm in Harvey method. The natural valence electron configuration calculations were analyzed by natural bond orbital. The distribution and contribution of the front molecular orbital of the initial complexes could be further understand by the density of states. The feature of the bonding evolution in the main pathways was studied using topological analysis including localized orbital locator and atoms in molecules.

**Keywords** Ethane · C-H bond activation · Dehydrogenation

## Introduction

In the past few decades, the activation of the C-H and C-C bonds in alkanes catalyzed by transition metal ions has attracted considerable attention, due to its importance and widespread application in the energy transform, organic synthesis, and catalytic researches [1–4]. In the previous studies, chemists have discovered that some mononuclear transition metal ions $M^+$ can activate the C-C and C-H bonds of alkanes. For example, methane could be activated by first-row and second-row transition metal cations [5, 6], C-C and C-H bonds of ethane activation by $Fe^+$ [7], etc. However, some mononuclear transition metal ions were not or low reactivity to the C-H bonds of alkanes. To solve this problem, chemists have attempted adding ligands to increase the catalytic efficiency of these metal ions. The catalytic efficiency of the metal was effectively enhanced by the synergy between the transition metal ion and the ligand. For instance, $Cr^+$ does not have any reactivity with small alkanes, whereas the diatomic $CrCl^+$ does [8]; and $CH_4$ cannot be activated by bare $Ni^+$, but $NiH^+$ brings about thermal bond activation [9]. Obviously, the metal combined with the ligand L by covalent bond changes considerably the catalytic activity of metals, and a suitably chosen ligand L can improve the reactivity of a reagent.

In 2007 and 2011, Schlangen et al. reported the reaction mechanism in gas-phase reactions of $NiX^+/RH$ couples (X = F, Cl, Br; R = $CH_3$, $C_2H_5$, $C_3H_7$, n-$C_4H_9$) in experimental section and theoretical aspects, respectively [10, 11]. As Ni congener, palladium is a precious metal, 0.0000015% abundance of palladium in the Earth's crust [12]. The reactivity of atomic palladium with alkanes was very low in the gas phase because its ground state cannot accomplish oxidative insertion, and its lowest excited state was also quite high in energy to deal with C-H bond activation [13]. Therefore, the addition of an appropriate ligand to enhance the catalytic activity of palladium had become an important issue. Compared with atomic Pd, theoretical studies and experiments have shown that the cationic palladium hydride has high activity toward C-H bonds of methane in the gas phase [14, 15]. Simultaneously, the dehydrogenation reaction of methane activation by $[Pd(H)(OH)]^+$ has been theoretically investigated at our

**Electronic supplementary material** The online version of this article (https://doi.org/10.1007/s00894-020-04357-w) contains supplementary material, which is available to authorized users.

✉ Zhi-Yuan Geng
zhiyuangeng@126.com

[1] College of Chemistry and Chemical Engineering, Northwest Normal University, Lanzhou 730070, Gansu, People's Republic of China

lab [16]. Theoretical studies on the activation of C-H bonds by $PdX^+$ (X = F, Cl, Br, H, and $CH_3$) had not been reported. To further insight into how halogen ligands affect the activity of palladium and the reaction mechanism with target molecules, in this paper, the reaction mechanism of $PdX^+$-activated ethane C-H bond was systematically studied theoretically.

## Computational methods

Theoretical calculation for all stationary points involved in the reaction of $PdX^+$(X = F, Cl, Br, H, and $CH_3$) with $C_2H_6$ has been surveyed by the density functional theory (DFT) [17–20]. For C, H, F, Cl, and Br, the large 6-311+G (d, p) basis set was applied [21]. The Pd atom was described by using the Stuttgart/Dresden relativistic effective core potentials (ECP) of SDD [22]. The vibrational frequency was calculated for each stationary point to confirm whether it was minima structure or transition state (TS). The minimum structure had only positive eigenvalues and TS had only one negative eigenvalue. Intrinsic reaction coordinate (IRC) calculations were performed to determine the correct link between the minima and the transition states (TS) [20]. The natural population analysis and the bonding properties for some structures have been made with natural bond orbital (NBO) analysis [23]. Density of states (DOS) of initial complexes was analyzed using the Multiwfn package [24, 25]. We used the single-point energy of the DFT to roughly locate crossing

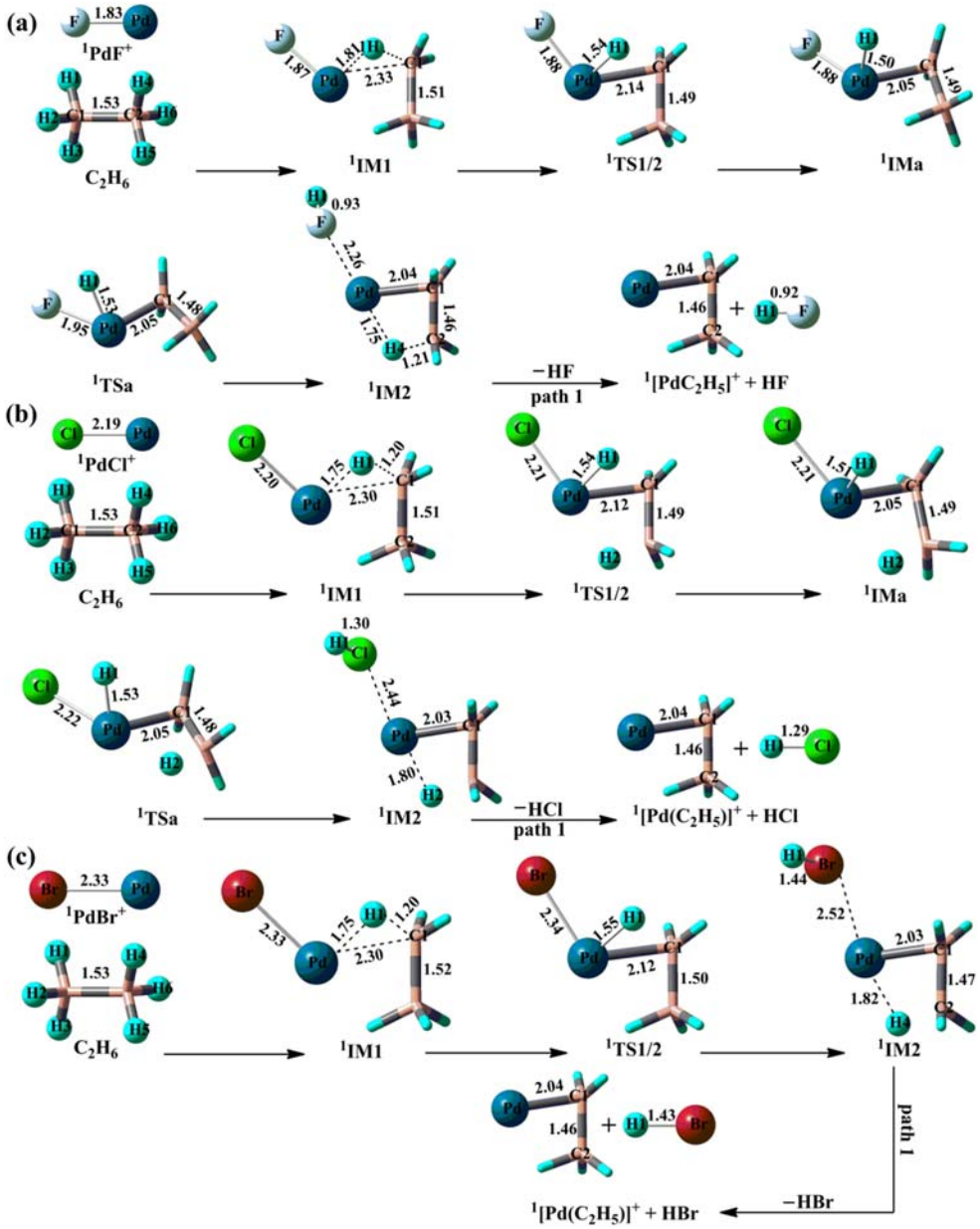


**Fig. 1** Optimized geometries for the stationary points of the first α-C-H bond activation of ethane in the singlet state (**a**) $^1PdF^+$, (**b**) $^1PdCl^+$, and (**c**) $^1PdBr^+$ (bond lengths unit Å)

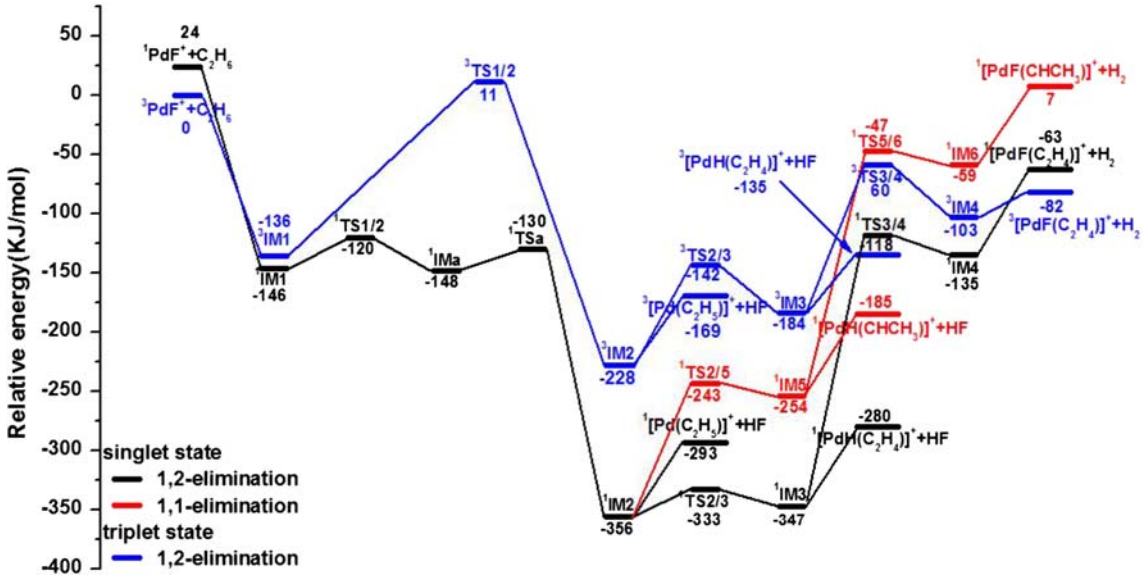


**Fig. 2** Potential energy profiles of reactions of ethane with $PdF^+$

points (CPs) between two potential energy surfaces (PESs). The minimum energy crossing point (MECP) was obtained using the mathematical algorithm proposed by Harvey et al. [26]. In addition, the bonding evolution of the main reaction pathways was studied by localized orbital locator (LOL) [27] analysis and atoms in molecules (AIM) [28] analysis using the Multiwfn program. All of the theoretical calculations were implemented using the Gaussian 09 program [29].

## Results and discussion

The mechanism of ethane activated by $PdX^+$ has been considered in singlet and triplet state. The superscript prefixes "1" and "3" were defined as the singlet and triplet states, respectively. The structures of stationary points in the high and low spin states and the corresponding PESs are depicted in Figs. 1, 2, 3, 4, 5, 6, 7, 8, 9, 10, and 11 (Fig. S1-S5 in support information). The scenario of the reaction paths is depicted in Scheme 1.

### Electronic structures of reactants

The calculated results showed that $^3PdX^+$ was ground state and the energy of $^3PdX^+$ (X = F, Cl, and Br) was 24, 57 and 102 kJ/mol lower than $^1PdX^+$, respectively. In contrast, $^1PdX^+$ was the ground state for $PdX^+$ (X = H and $CH_3$). The energy of the triplet state $^3PdX^+$ was 82 and 88 kJ/mol higher than the

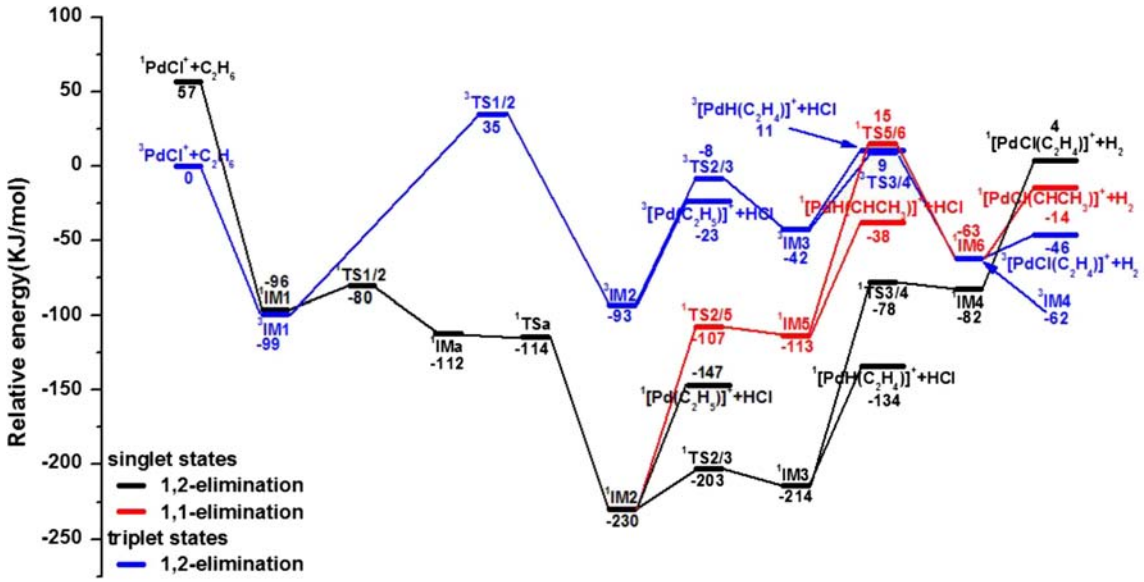


**Fig. 3** Potential energy profiles of reactions of ethane with $PdCl^+$

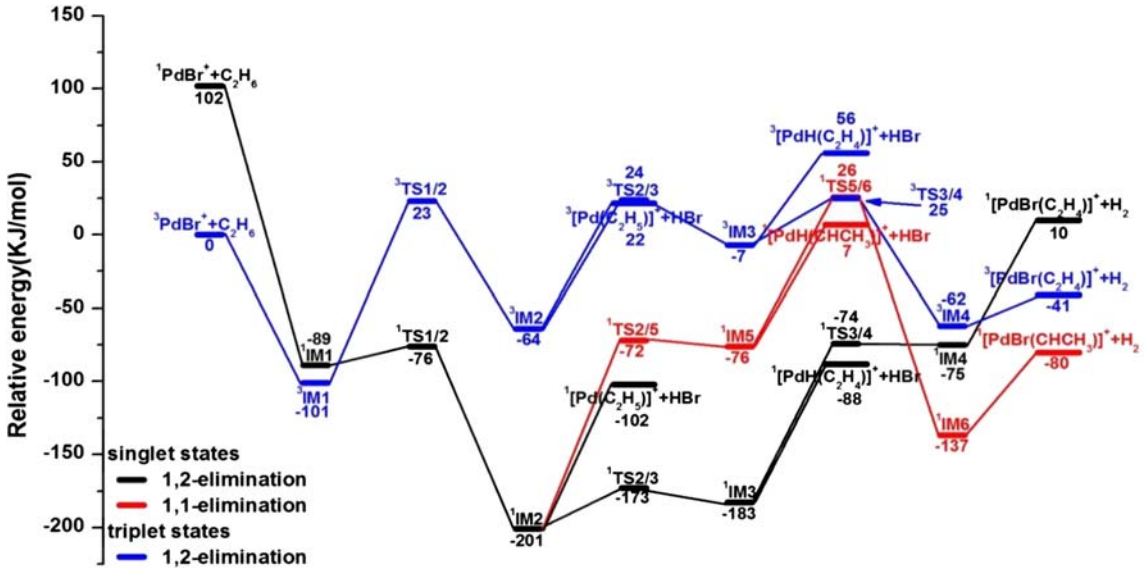


**Fig. 4** Potential energy profiles of reactions of ethane with $PdBr^+$

ground state, respectively. The energy level differences of the reactants between the singlet and triplet state became gradually bigger from $PdF^+$ to $PdCl^+$ and $PdBr^+$, while $PdH^+$ was very close to those of the $PdCH_3^+$. The natural valence electron configuration calculations were performed for $PdX^+$ (X = F, Cl, Br, H, and $CH_3$), which is shown in Table 1. From F to $CH_3$, the electronic number of the 4d orbital was increased significantly, and the 5s orbit had almost no changed in the singlet state. In contrast, the number of 5s orbital electrons was changed obviously, whereas the 4d orbital did not in the triplet state.

As shown in Fig. 1 and Fig. S1, the bond distances of $PdX^+$ (X = F, Cl, Br, H, and $CH_3$) were 1.83, 2.19, 2.33, 1.48, and 1.99 Å (in the singlet state) and 1.88, 2.22, 2.32, 1.58, and 2.15 Å (in the triplet state), respectively. From H to Br, the distance of the Pd-X (H < F < $CH_3$ < Cl < Br) bond gradually increased. The change in the bond distance of $PdX^+$ was explained by the atomic radius increase from H to Br. From Figs. 1 and 7 (Fig. S1-S5), one can see that the bond distances of the low spin state $PdX^+$ ions were shorter than the high spin state. The bond distance for $PdX^+$ was determined by the spatial extent of the valence orbit (5s and 4d) [30]. The NBO analysis results indicated that the Pd-X bond was mainly composed of the p orbital of X with the 5s and 4d orbitals of palladium. However, since the less electron in 5s orbital of Pd in $^1PdX^+$, the bond distance of Pd-X in the low spin state was shorter than that in the high spin state.

## Initial complexes

The reaction started from catalyst $PdX^+$ (X = F, Cl, Br, H, and $CH_3$) combined with ethane to yield initial complexes IM1, in which the primary C-H bond was elongated (1.09 Å for free ethane), as shown Table 2. The binding energies of the formation of the initial complexes were 170, 153, 191, 102, and 70 kJ/mol (in singlet states) and 136, 99, 101, 62, and 77 kJ/mol (in triplet states), respectively. The initial complexes IM1 was found to had a $\eta^3$ coordination, as seen Figs. 1 and 7, and Fig. S1-S5. Based on the distance of the activated C-H and the corresponding Pd-C in the initial complexes IM1 (see Table 2), it was concluded that there was an agostic Pd···H-C interaction prior to C-H cleavage.

To better understand the molecular orbital composition, we performed DOS analysis of initial complexes M1 (see Fig. S6) [31]. In the picture, fragment 1, fragment 2, fragment 3, and fragment 4 represented carbon, hydrogen, palladium, and ligand, respectively. The vertical dashed line indicated the position of HOMO level. The height of black curve represented the total density of states (TDOS), and we could clearly see the density of the energy levels distributed and strength everywhere. The curve of the partial density of states (PDOS) was valuable for visualizing the contribution of each atomic orbital (AO) to the molecular orbital (MO). For example, the PDOS-Pd curve was relatively high and close to the TDOS in the region of HOMO level, respectively. Therefore, we concluded that the d orbital of palladium had great contribution to the HOMO orbits.

## Reaction mechanisms

### Reactivities of $PdX^+$ (X = F, Cl, and Br) with $C_2H_6$

Before the transition state $^3$TS1/2, there was a crossing phenomenon between the two PESs, as show in Figs. 2, 3, and 4. After the cross points, the reaction was carried out along the single PES in a spin-conserving manner. Since the stationary points of the triplet state were higher in energy than those of the singlet state, we were not going to discuss the triplet state

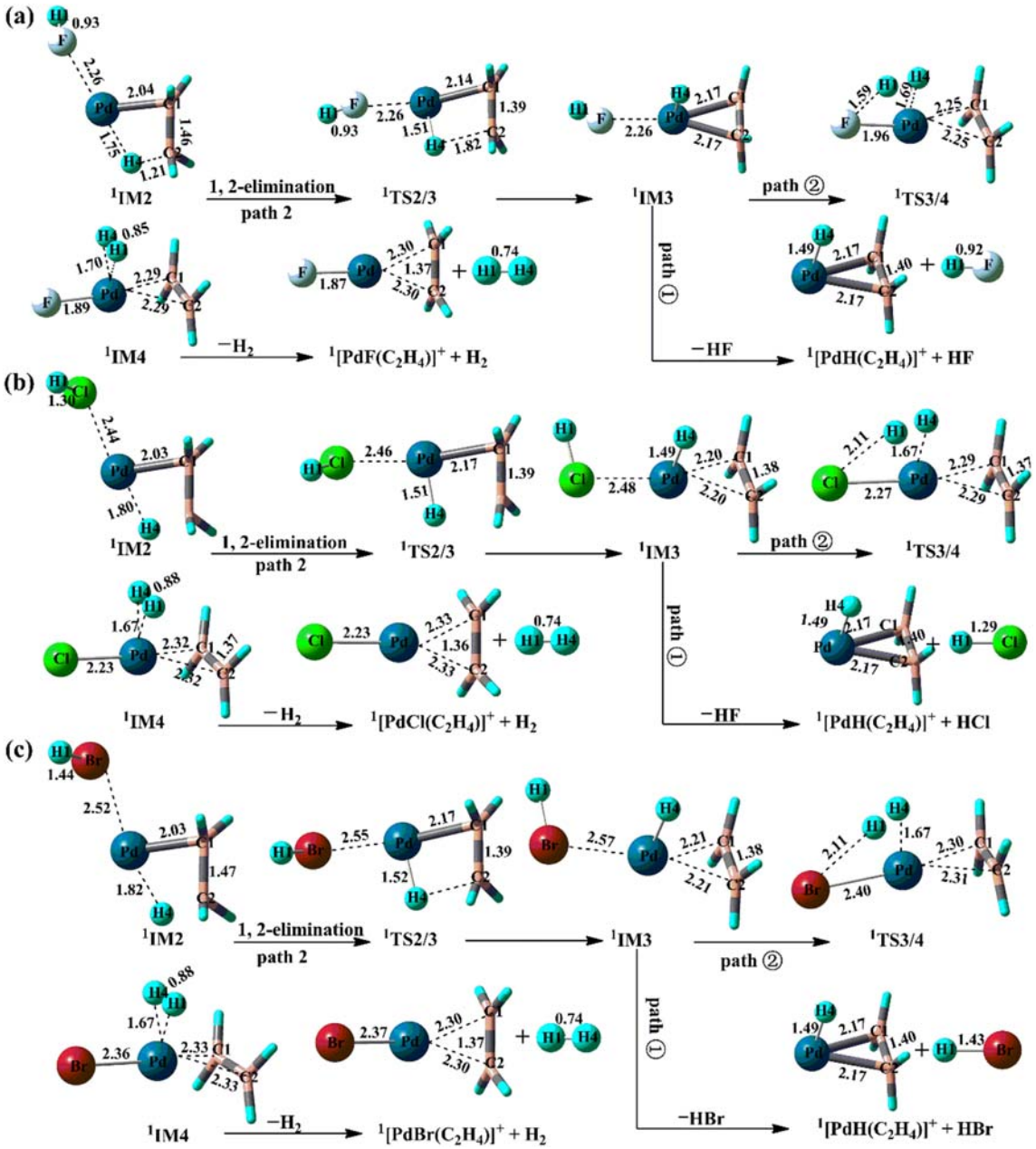


**Fig. 5** Optimized geometries for the stationary points of the β-C-H bond activation of ethane in the singlet state (**a**) $^1PdF^+$, (**b**) $^1PdCl^+$, and (**c**) $^1PdBr^+$ (bond lengths unit Å)

PES further. Starting with the initial complexes IM1, the hydrogen atom H1 transferred from the α-carbon of ethane to $PdX^+$ and afforded an intermediate $^1$IM2. In this process, H1 was transferred in two different ways (see Fig. 1).

In one, H1 shifted to palladium from ethane via the three-centered late transition state $^1$TS1/2, resulted the high-energy intermediate $^1$IMa in $^1PdX^+/C_2H_6$ (X = F, Cl) system. In $^1$IMa, the distance of the Pd-H bond was 1.50 Å, and NBO analysis revealed that the Pd-H1 bond was formed from 5s and $4d_{z^2}$ orbital of palladium and 1s orbital of hydrogen (see Fig. S7). After this oxidation addition (OA) reaction, the hydrogen atom migrated from palladium to halogen through reductive elimination (RE), and the stable intermediate $^1$IM2 ($FHPd(C_2H_5)^+$ and $ClHPd(C_2H_5)^+$) was formed. The exothermicity of the whole OA/RE process was 210 and 131 kJ/mol, respectively. In addition, the transition state $^1$TSa was −114 kJ/mol lied below intermediate $^1$IMa by 2 kJ/mol when the zero-point energy correction was taken into account in $^1PdCl^+/C_2H_6$ (see Fig. 3), indicated that the process was a low-barrier or even barrier-free transformation on the overall low spin reaction path. Another way, in $^1PdBr^+/C_2H_6$, the hydrogen atom H1 shifted directly to form the intermediate $^1$IM2 via transition state $^1$TS1/2 with a barrier of 25 kJ/mol; this step was exothermic by 112 kJ/mol. In the process of σ-

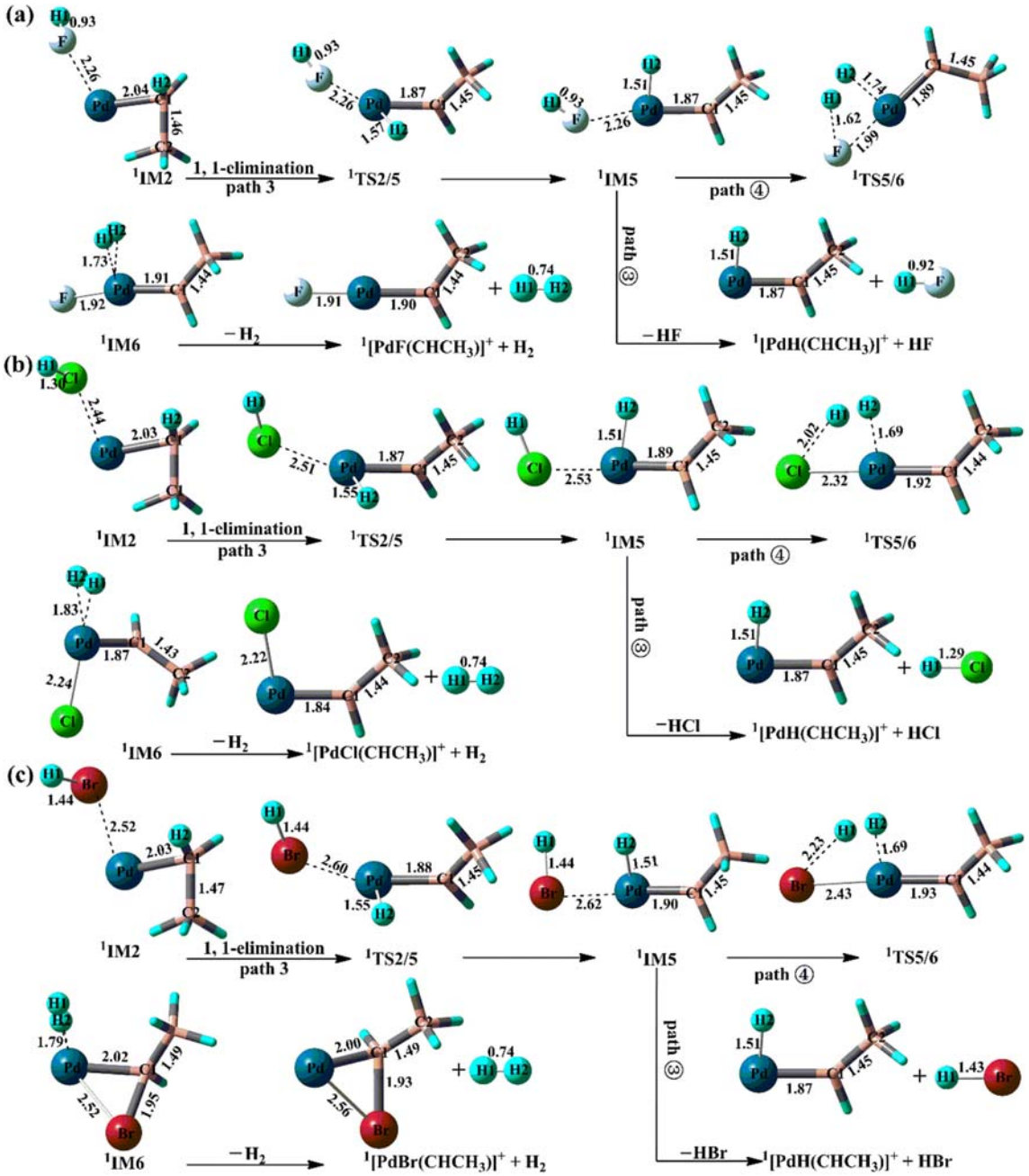


**Fig. 6** Optimized geometries for the stationary points of the second α-C-H bond activation of ethane in the singlet state (**a**) $^1PdF^+$, (**b**) $^1PdCl^+$, and (**c**) $^1PdBr^+$ (bond lengths unit Å)

CAM, the Pd-X and C1-H1 bonds are concurrently broken, and two σ-bonds of Pd-C1 and X-H1 were formed simultaneously. In $^1$IM2, the Pd-C1 and C1-C2 bond lengths were 2.04 and 1.46 Å, respectively. This variation remained almost constant across from F to Br. But the Pd-X bond trends to lengthen along from F to Br. The intermediate $^1$IM2 was the global minimum structure on the singlet potential energy surface, and the energy of $^1$IM2 relative to the ground state reactants was − 356, − 230 and − 201 kJ/mol, respectively. As shown in Fig. 12, the π orbital of the four-membered ring was formed from p orbital of two C atoms and d orbital of Pd in $^1$IM2. This interaction results in increased stability of the intermediate $^1$IM2. After intermediate $^1$IM2, the reaction was divided into three paths, as shown in Scheme 1. Path 1, the loss of HX directly in the intermediate $^1$IM2 required energy of 63, 83, and 99 kJ/mol, respectively, yielded metal ethyl ions $^1Pd(C_2H_5)^+$. The exothermicity of the loss of HX gradually decreased from F to Br relative to ground state reactants. Path 2 and 3 channels were distinguished based on the reaction mechanism of 1, 2- and 1, 1-elimination of hydrogen. The following reaction mechanism of path 2 and 3 was discussed in detail.

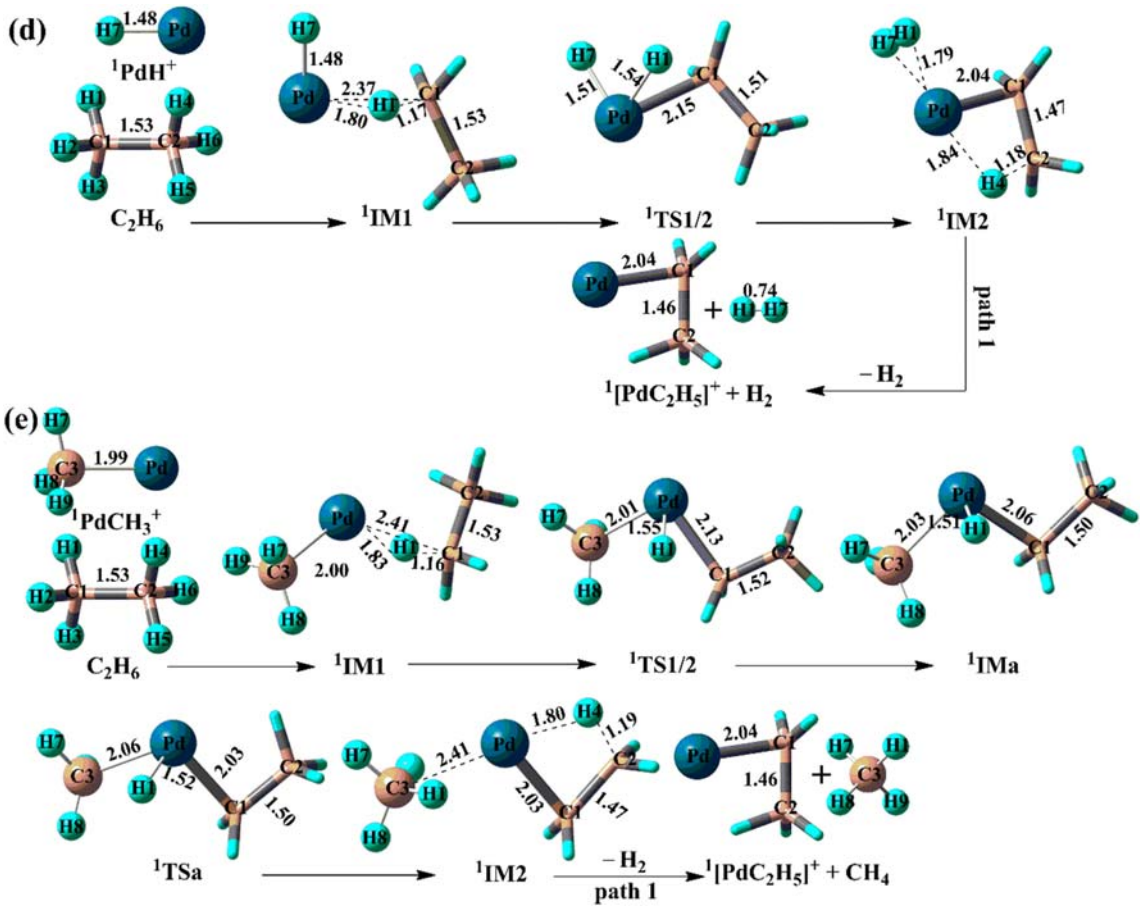


**Fig. 7** Optimized geometries for the stationary points of the first α-C-H bond activation of ethane in the singlet state (**d**) $^1PdH^+$ and (**e**) $^1PdCH_3^+$ (bond lengths unit Å)

**1, 2-Elimination mechanism** The second hydrogen atom H4 from β-carbon on the ethyl ligand shifted to the palladium via a four-member (Pd-C1-C2-H4) transitional structure $^1$TS2/3, given rise to the hydride complex $^1$IM3 (see Fig. 5). The second C-H activation energy barriers were 23, 27, and 28 kJ/mol, respectively. In intermediate $^1$IM3, the Pd, $C_1$, and $C_2$ atom formed an isosceles triangle. In the step, the distance of the C-C was shortened from 1.53 Å in

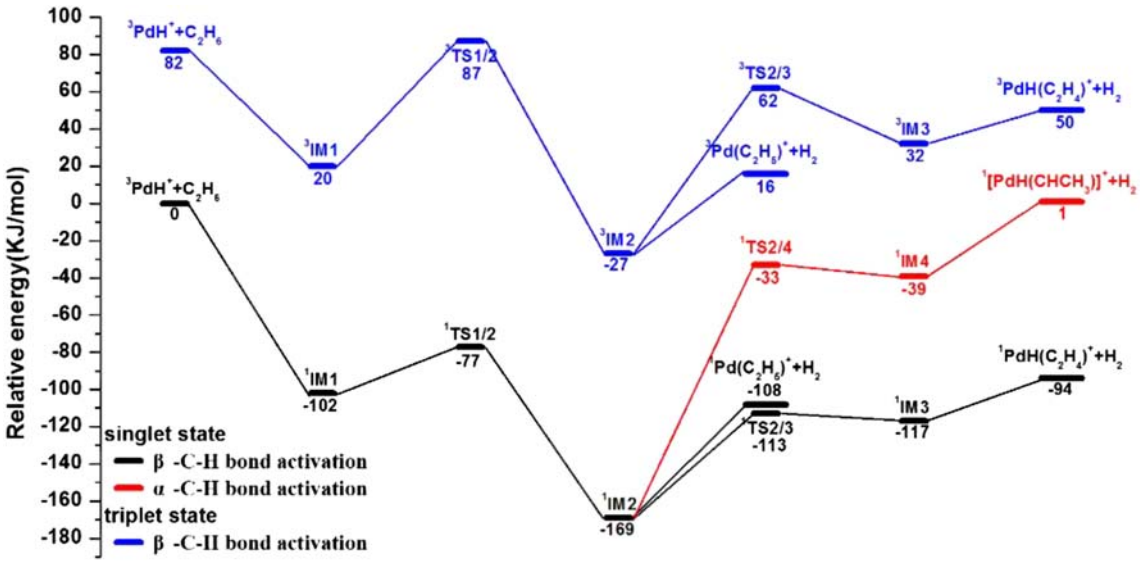


**Fig. 8** Potential energy profiles of reactions of ethane with $PdH^+$

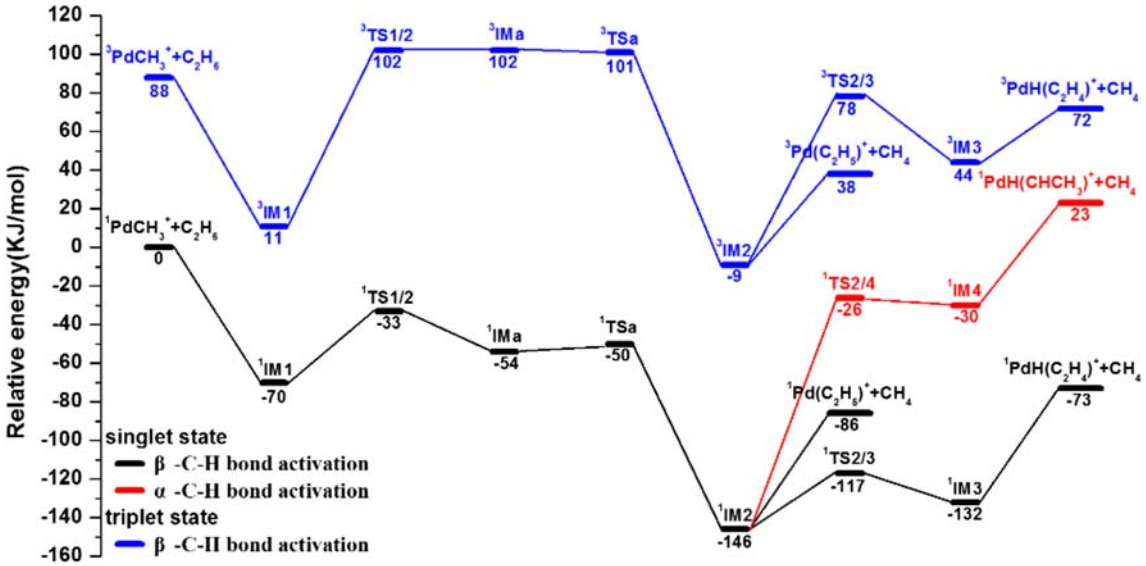


**Fig. 9** Potential energy profiles of reactions of ethane with $PdCH_3^+$

an isolated ethane molecule to 1.38 Å. The changed of distance suggested that the C-C double bond has been formed (the distance of C-C bond in ethylene molecules was 1.33 Å). This step was endothermic by 9, 16, and 18 kJ/mol, respectively.

After the formation of the intermediate $^1$IM3, the reaction bifurcated to two routes (see Scheme 2). One route was the expulsion of HX directly from the newly formed complex $^1$IM3 with an activation barrier of 67, 80, and 95 kJ/mol, respectively. Another route was H1 back transfer from HX to the hydride ligand via transitional structure $^1$TS3/4 to afford the $^1$IM4 molecular complexes, as path ②. The energy barrier value in this step was 229, 136, and 109 kJ/mol, respectively. Compared with the loss of HX, dehydrogenation was relatively difficult. The reason was that the d orbital of the Pd in $PdX^+$ interacted with the π orbital of the C=C bond and formed π bond in intermediate $^1$IM3 (see Fig. S9). In order to reach $^1$TS3/4, the intermediate $^1$IM3 needed to overcome more energy. And the energy barrier gradually decreased from F to Br relative to $^1$IM3. In the reaction mechanism of σ-CAM, Pd-H4 and X-H1 bonds were concurrently broken and then H-H and Pd-X bonds were formed simultaneously. The $H_2$ elimination process was endothermic by 212, 132, and 108 kJ/mol, respectively. Finally, the elimination of $H_2$ from the newly yielded $^1PdX(H_2)(C_2H_4)^+$ complex terminated this reaction pathway. In this process, it is necessary to overcome the dissociation energies of 72, 86, and 85 kJ/mol, respectively. Dehydrogenation was the rate-determining step of path 2. The final products of the reaction of $PdX^+$ with ethane were the mixture of HX and $H_2$.

**1, 1-Elimination mechanism** In the second hydrogen transfer process, there was competition between α-hydrogen and β-

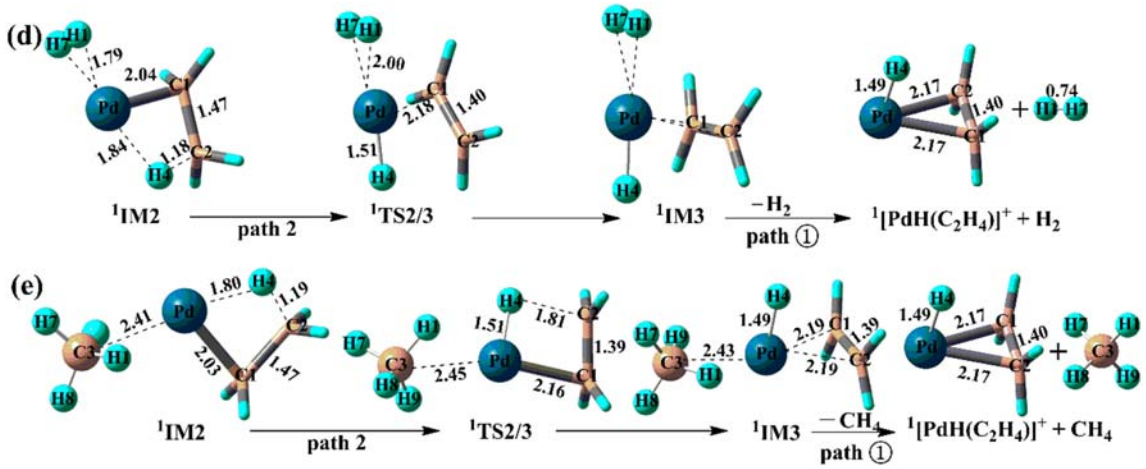


**Fig. 10** Optimized geometries for the stationary points of the β-C-H bond activation of ethane in the singlet state (**d**) $^1PdH^+$ and (**e**) $^1PdCH_3^+$ (bond lengths unit Å)

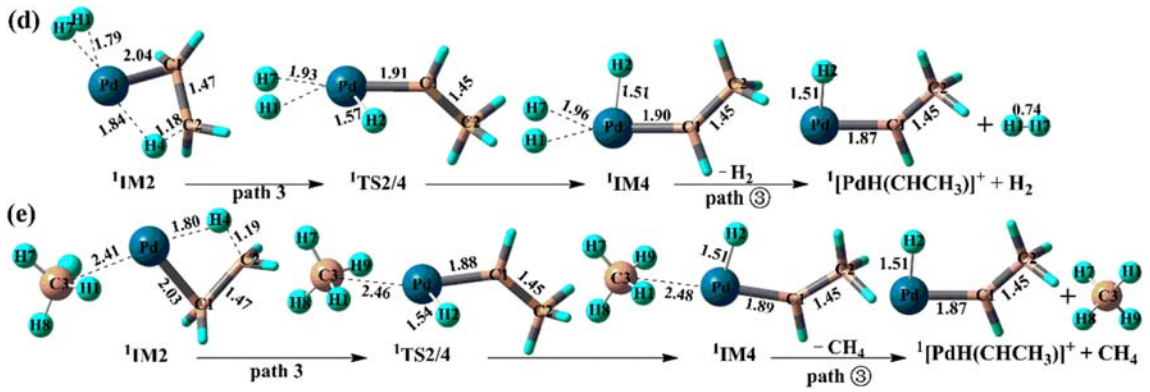


**Fig. 11** Optimized geometries for the stationary points of the second α-C-H bond activation of ethane in the singlet state (**d**) $^1PdH^+$ and (**e**) $^1PdCH_3^+$ (bond lengths unit Å)

hydrogen on the ethane. For the path 3, starting from the intermediate $^1$IM2, the second hydrogen atom H2 from the α-carbon migrated to palladium via transition state $^1$TS2/5, which lead to intermediate $^1$IM5 (see Fig. 6). H2 transfer occurred with the activation barrier of 113, 123, and 129 kJ/mol, respectively. The step was endothermic by 101, 117, and 125 kJ/mol, respectively.

Subsequently, the reaction was divided into two paths (see Scheme 3). In path ③, HX was liberated directly and $^1Pd(H)(CHCH_3)^+$ was formed by overcoming an activation barrier of 69, 75, and 83 kJ/mol, respectively. In path ④, H1 from HX back transferred to the hydride ligand via transition state $^1$TS5/6, and then an intermediate $^1$IM6 was formed. Corresponded activation barriers were 229, 136, and 109 kJ/mol, respectively. We noted in particular the features of the transition structure $^1$TS5/6 in which the migrated H1 atom interacted with three centers simultaneously, that is, the palladium, halogen, and H2 atoms. As required for an σ-CAM process, the atoms H1, H2, Pd, and X (X=F, Cl, Br) were coplanar in $^1$TS5/6. A similar trend was seen in the $^1BrPd(C_2H_6)^+ \rightarrow {}^1(HBr)Pd(C_2H_5)^+$ and $^1$IM3 → $^1$IM4 transformation. Here, the H-H bond distance was 0.85 Å, which was very close to H-H bond distance (0.74 Å) of free $H_2$. It was suggested that the Pd-H2 and H1-X bonds were broken and H-H bond was formed. During this reaction, dehydrogenation was the rate-determining step. In the last step, $H_2$ and $^1$XPd (CHCH3)$^+$ were formed by overcoming 66, 49, and 57 kJ/mol dissociation energy, respectively. In the following section, we would discuss the reaction of $PdH^+$ and $PdCH_3^+$ with $C_2H_6$ in detail.

## Reactivities of $PdX^+$ (X = H and $CH_3$) with $C_2H_6$

In the reaction of $PdH^+$ and $PdCH_3^+$ with $C_2H_6$, the reaction mechanism and optimized structures on the two PESs were very similar to those for the reaction of $PdX^+/C_2H_6$ (X = F, Cl, and Br) discussed above. Unlike $PdF^+$, $PdCl^+$, and $PdBr^+$, the whole reaction of $PdH^+$ and $PdCH_3^+$ with $C_2H_6$ proceeded on the ground state PES in a spin-conserving manner. Similar to $PdX^+$ (X = F, Cl, and Br), we only discuss the reaction mechanism on the ground state PESs. Starting with the initial complexes $^1$IM1, the hydrogen atom H1 transferred from ethane to $PdX^+$ in two ways and to yield an intermediate $^1$IM2. In the process of the C-H1 bond activation, there was no low energy barrier $^1$IMa → $^1$TSa → $^1$IM2 process on the $^1PdH^+/C_2H_6$, whereas the barrier was 6 kJ/mol on the $^1PdCH_3^+/C_2H_6$. H1 transferred in $^1PdCH_3^+$ was very similar to that of $^1PdF^+$ and $^1PdCl^+$, with a total exothermicity of 76 kJ/mol, while $^1PdH^+$ and $^1PdBr^+$ were similar, this process exothermic 67 kJ/mol.

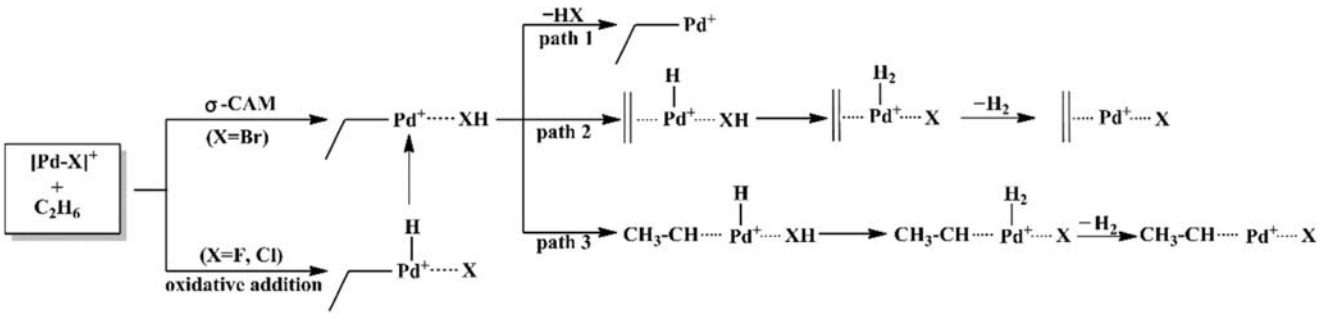


**Scheme 1** The scenario of the reaction paths

**Table 1** Valence natural bond orbital population of Pd on the $PdX^+$ complexes

| Species | Singlet | Triplet |
|---|---|---|
| $PdF^+$ | $5s^{0.02}4d^{8.65}5p^{0.03}$ | $5s^{0.06}4d^{8.61}5p^{0.02}$ |
| $PdCl^+$ | $5s^{0.18}4d^{8.85}5p^{0.03}$ | $5s^{0.11}4d^{8.89}5p^{0.03}$ |
| $PdBr^+$ | $5s^{0.20}4d^{8.94}5p^{0.04}$ | $5s^{0.21}4d^{8.91}5p^{0.04}$ |
| $PdH^+$ | $5s^{0.08}4d^{9.12}5p^{0.01}$ | $5s^{0.37}4d^{8.64}5p^{0.01}$ |
| $PdCH_3^+$ | $5s^{0.02}4d^{9.20}5p^{0.01}$ | $5s^{0.33}4d^{8.74}5p^{0}$ |

The intermediate $^1$IM2 was the global minimum structure on the whole PESs, which was 169 and 146 kJ/mol below the ground state reactants, respectively. After overcoming 61 kJ/mol in the $^1PdH^+$ and 60 kJ/mol in the $^1PdCH_3^+$, $H_2$ and $CH_4$ were liberated. For the second C-H bond activation in the $^1PdH^+/C_2H_6$ and $^1PdCH_3^+/C_2H_6$, there was also competition between α-H and β-H similar to that in the reaction of $^1PdF^+$, $^1PdCl^+$, and $^1PdBr^+$ with ethane (path 2 and 3).

The β-C-H and the second α-C-H bond activation occurred in the same way as that of $^1PdF^+$, $^1PdCl^+$, and $^1PdBr^+$. $^1$IM2 → $^1$TS2/3 → $^1$IM3 was the β-C-H bond activation process with the activation barrier of 56 and 29 kJ/mol, respectively. The step was endothermic by 52 for $^1PdH^+$ and 14 kJ/mol for $^1PdCH_3^+$. Similar to $^1PdX^+/C_2H_6$ (X = F, Cl, and Br), the Pd, C1, and C2 atom was an isosceles triangle in intermediate $^1$IM3. Finally, $H_2$ and $CH_4$ were liberated from $^1$IM3 with an activation barrier of 23 and 59 kJ/mol, respectively.

$^1$IM2 → $^1$TS2/4 → $^1$IM4 was the second α-C-H bond activation process. The C-H activation occurred with the activation barrier of 136 and 120 kJ/mol, respectively. The step was endothermic by 130 and 116 kJ/mol, respectively. Subsequently, $H_2$ and $CH_4$ were liberated directly, and $^1Pd(H)(CHCH_3)^+$ was formed by overcoming dissociation energy of 40 and 53 kJ/mol, respectively. Similarly, the activation of β-C-H bond was also easier than that of the second α-C-H bond in $^1PdH^+$ and $^1PdCH_3^+$. However, for $PdX^+/C_2H_6$ (X = H and $CH_3$), the hydrogen atom H1 back transfer from HX to the hydride ligand and combined with H2 or H4 on Pd to afford $H_2$ was not observed. In paths 1 and 2, the energy of all points on the singlet state was lower than those of the reactants, indicated that these reactions were a barrier-free transformation. In path 3, the whole reaction was only endothermic 1 kJ/mol for $^1PdH^+$ and 2 kJ/mol for $^1PdCH_3^+$. The final product was $H_2$ for $PdH^+$ and $CH_4$ for $PdCH_3^+$.

**Table 2** Computed bond distances r(C-H), r(Pd-H), and r(Pd-C) for the $PdX(C_2H_6)^+$ complexes

| species | r(C-H) (Å) | | r(Pd-H) (Å) | | r(Pd-C) (Å) | |
|---|---|---|---|---|---|---|
| | $^1\Sigma$ | $^3\Sigma$ | $^1\Sigma$ | $^3\Sigma$ | $^1\Sigma$ | $^3\Sigma$ |
| $PdF(C_2H_6)^+$ | 1.18 | 1.14 | 1.81 | 2.01 | 2.33 | 2.48 |
| $PdCl(C_2H_6)^+$ | 1.20 | 1.13 | 1.75 | 2.06 | 2.30 | 2.54 |
| $PdBr(C_2H_6)^+$ | 1.20 | 1.13 | 1.75 | 2.08 | 2.30 | 2.59 |
| $PdH(C_2H_6)^+$ | 1.17 | 1.12 | 1.80 | 2.10 | 2.37 | 2.64 |
| $PdCH_3(C_2H_6)^+$ | 1.16 | 1.15 | 1.83 | 1.91 | 2.41 | 2.49 |

## Rate constant

From the potential energy profiles in Figs. 2, 3, and 4, it could be seen that the rate-determining transition $^1$TS3/4 was located below $^1$TS5/6 in the process of 1, 2-elimination in reaction of $^1PdX^+$ (X = F, Cl, Br) with ethane. Compared with β-hydrogen transfer in pathway 2, the process of α-hydrogen in the pathway 3 had less competitive ability. And the process of HX loss was relatively easier than $H_2$ elimination in the whole pathway 2. In $^1PdX^+/C_2H_6$ (X = H, $CH_3$) system, path 2 was also more favorable than path 3, as shown in Figs. 8 and 9. To estimate quantitatively the reactivity for several product formation processes of path 2 (Pd-X bond cleavage products, $^1Pd(C_2H_5)^+$ + HX and $^1PdH(C_2H_4)^+$ + HX, and without apparent Pd-X bond cleavage products $^1PdX(C_2H_4)^+ + H_2$), the rate constants have been evaluated based on conventional transition state theory (Eq. (1)) [32].

$$k(T) = \frac{k_B T}{h} \exp\left(-\frac{\Delta G^{\neq}}{RT}\right) \quad (1)$$

where $k_B$ is the Boltzmann constant, $T$ is the thermodynamic temperature, $h$ is the Plank constant, and $\Delta G^{\neq}$ is the activation Gibbs free energy barrier. In $T = 298$ K, the rate constants of the rate-determining step in several products formation process have been calculated in Table 3.

Compared with the rate constants in several product formation processes, we concluded that the rate constant gradually decreased in the loss HX while gradually increases in the $H_2$ elimination from F to Br. The results showed that the loss of HX was most favorable for $^1PdF^+/C_2H_6$, but the elimination of $H_2$ was easier for $^1PdBr^+/C_2H_6$. In $^1PdX^+/C_2H_6$ (X = H and $CH_3$), only the products of Pd-X bond cleavage were observed. Also, the dissociation of product $^1PdH(C_2H_4)^+$ + HX was easier than that of product $^1Pd(C_2H_5)^+$ + HX.

To intuitively illustrate the efficiency of HX and $H_2$ elimination, branching ratios of all products were presented. As shown in Fig. 13, the loss of HX was abundant for all systems, whereas the elimination of $^1PdX(C_2H_4)^+ + H_2$ was relatively most effective for $^1PdBr^+/C_2H_6$. This was consistent with the results of the discussion above.

Gas-phase reactions proceed in closed containers, and all of these reactions occur at constant energy and angular momentum. Depuy reports, in the gas phase, the reaction that occurred through an ion-dipole complex that contains high energy [33]. In the reaction of $PdX^+$ with ethane, the formation of encounter complex IM1 in the minimal energy reaction pathways (MERPs) contributed 146, 99, 101, 102, and

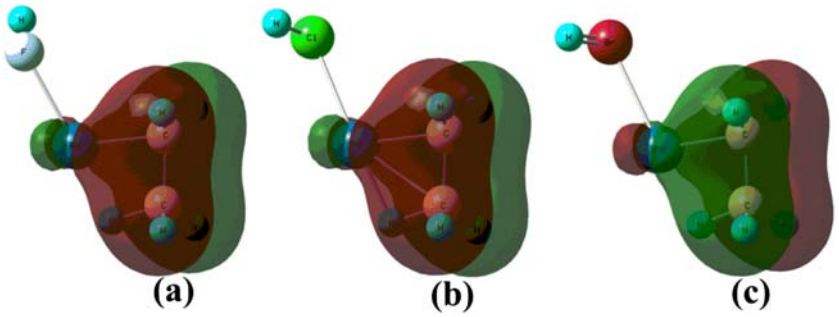


**Fig. 12** Orbital interaction diagram at the four-membered ring (Pd-C1-C2-H4) in intermediate $^1$IM2 (**a**) $^1PdF^+$, (**b**) $^1PdCl^+$, and (c) $^1PdBr^+$

70 kJ/mol (for F, Cl, Br, H, and $CH_3$) of heat to the closed system, respectively. And all energies were retained within the encounter complex IM1 since there were no solvent molecules to transfer it. This indicated that there was enough energy to overcome the reaction barrier. Therefore, we concluded from the above calculation results that ethane was effectively activated by $PdX^+$ at room temperature.

## MECP between PESs of different multiplicities

As shown in Figs. 2, 3, and 4, the crossing phenomenon between two PESs was observed at both the entrance and exit channels of reaction of $PdX^+$ (X = F, Cl, and Br) with ethane. In $PdF^+/C_2H_6$, the energy of $^3$IM1 was higher than $^1$IM1 by 10 kJ/mol, which implied that CPs existed at the entrance channel of reaction. For $PdCl^+$ and $PdBr^+$, the energy of $^3$IM1 was 3 and 12 kJ/mol lower than that of $^1$IM1, while $^3$TS1/2 was higher than $^1$TS1/2 by 115 and 99 kJ/mol, respectively, which indicated that CPs existed between $^3$IM1 and $^3$TS1/2. From Br to F, CPs was gradually close to the reactants. In order to locate the CPs between two PESs, we used the method of partial geometry optimization to calculate single-point energy. To more accurately locate the CP, the method of Harvey et al. was used to obtain the actual MECP, as shown in Fig. 14. This change of spin states between two PESs effectively avoided the energetically inaccessible transition structure $^3$TS1/2 on the ground state surface. This spin-crossing phenomenon could be called a "two-state reaction" in the organometallic chemistry [34]. After the systems crossing, the whole reaction on the singlet PESs proceeded in a spin-conserving manner. The minimal energy reaction pathway (MERP) started from the triplet state reactants via intersystem crossing mechanism, then proceeded along the low spin PESs to liberate HX and $H_2$. For $PdX^+/C_2H_6$ (X = H, $CH_3$), the whole reaction proceeded in a spin-conserving manner on the singlet PESs, and there was no crossing phenomenon, as shown in Figs. 8 and 9.

## Bonding evolution analysis

To further understand bond evolution of the main reaction pathways, LOL and AIM analyses were investigated. LOL was a function for locating high localization regions, defined by Schmider and Becke. Compared with the electron localization function (ELF) [35], LOL has similar description. Jacobsen reported that LOL could exhibit more accurate and clearer picture than ELF [36]. The value range of LOL is (0, 1). The LOL pictures for the stationary points in main paths were described in Fig. 15 and Fig. S11–12. The regions of white in pictures indicated that electron density exceeded the upper limit of color scale (0.8). In AIM analysis, the chemical bonding was described by the bond critical point (BCP) [37]. The bond strength and the atomic interaction at BCP were estimated by the electron density ($\rho_b$) and the Laplacian electron density ($\nabla^2\rho_b$), respectively. BCP has been analyzed in terms of the values of $\rho_b$ and $\nabla^2\rho_b$ at the (3, − 1) critical points. The values of $\rho_b$ and $\nabla^2\rho_b$ were listed in Table S1–5. Positive and negative values of $\nabla^2\rho_b$ indicated that electron density was depleted and concentrated.

As shown in Fig. 15 and Fig. S11-S12, the low LOL value indicated that there was no covalent bond between Pd and H1 atom in $^1$IM1. This conclusion was confirmed by the AIM analysis; result showed that $\rho_b$ between Pd and H1 atom was very low ($\rho_b$ = 0.078, 0.088, 0.088, 0.079, and 0.70 au, respectively), and $\nabla^2\rho_b$ value was positive. The first C-H bond was activated in two different ways. For F, Cl, and $CH_3$, the LOL of $^1$TS1/2

**Scheme 2** 1, 2-Elimination reaction paths

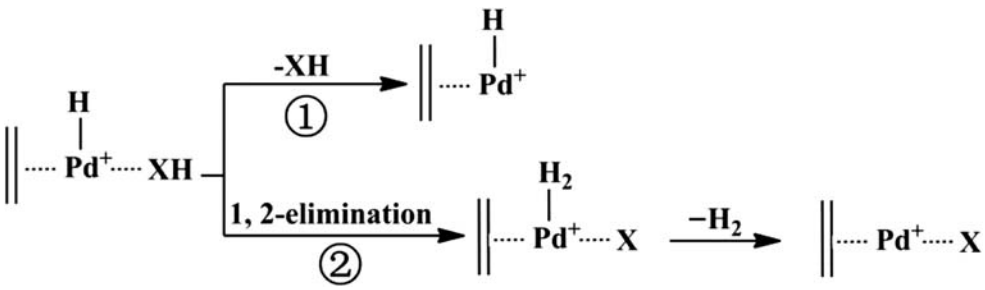

**Scheme 3** 1, 1-Elimination reaction paths

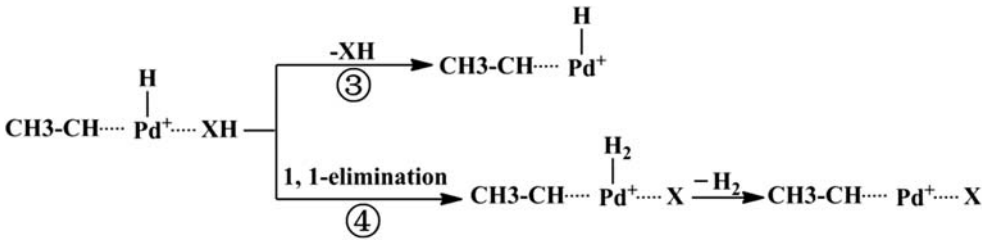


showed that C1-H1 bond was broken and Pd-H1 bond begins to form. In $^{1}$TS1/2, the $\rho_b$ of Pd-H1 bond significantly increased ($\rho_b$ = 0.152, 0.150, and 0.152 au, respectively), and $\nabla^2\rho_b$ of Pd-H1 bond was negative value, but the Pd-H1 bond was not yet formed. In intermediate $^{1}$IMa, Pd-H1 bond was completely formed. This is consistent with the AIM analysis, which showed that $\rho_b$ values of Pd-H1 bond were 0.171, 0.166, and 0.166 au respectively. Compared with $^{1}$IMa, the $\rho_b$ value of Pd-H1 and Pd-X was decreased while Pd-C1 increased in $^{1}$TSa, indicated that H1 was transferred from Pd to ligand. In $^{1}$TSa, AIM analysis showed that the $\rho_b$ value of Pd-H1 bond was 0.152, 0.157, and 0.158, respectively; this result indicated that the Pd-H1 bond was broken. Another for Br and H, H1 was transferred directly from C1 to Br and H, respectively. AIM analysis showed that the $\rho_b$ (0.148 and 0.151 au) of Pd-H1 in $^{1}$TS1/2 increased obviously compared with that in $^{1}$IM1. Subsequently, the second C-H bond was activated. In $^{1}$TS2/3, the $\rho_b$ value of Pd-H4 increased obviously compared with $^{1}$IM2, and $\nabla^2\rho_b$ was negative value, suggested that H4 atom was gradually transferred from C2 to Pd. In addition, the weak interaction between Pd and H4 also was observed in $^{1}$IM2, which was confirmed by the small $\rho_b$ value ($\rho_b$ = 0.087, 0.079, 0.075, 0.072, and 0.078 au, respectively). In $^{1}PdX^{+}/C_2H_6$ (X = H and $CH_3$), the reaction was terminated after the formation of intermediate $^{1}$IM3. In the $^{1}PdX^{+}/C_2H_6$ (X = F, Cl, and Br) system, the $\rho_b$ value of the H1-H4 bond was 0.180~0.186 au, indicated that $H_2$ was formed in stage of $^{1}$TS3/4. The H1-H4 bond was formed completely in $^{1}$IM4; this was also confirmed by the AIM analysis.

## Comparison the reactivity of $PdX^{+}$(X = F, Cl, Br, H, and $CH_3$) with atomic Pd and $Pd^{+}$ toward $C_2H_6$ activation

In order to compare the reactivity of Pd, $Pd^{+}$, and $PdX^{+}$ with ethane, we theoretically studied the reaction mechanism of Pd and $Pd^{+}$ with ethane at the same level as $PdX^{+}$. The optimized structure of stable point on PESs of two spin states is shown in Fig. S13-S14. The calculated results showed that the ground states were $^{1}$Pd and $^{2}Pd^{+}$, respectively. The energy of the excited state $^{3}$Pd and $^{4}Pd^{+}$ was 79 and 277 kJ/mol higher than the ground states, respectively. The NBO valence electron populations of the high spin were calculated to be $5s^{1.00}4d^{9.00}$ and $5s^{1.00}4d^{8.00}$ for $^{3}$Pd and $^{4}Pd^{+}$, respectively. In the reaction of atom Pd with $C_2H_6$, $C_2H_6$ cannot been activated by triplet $^{3}$Pd, because of its lowest excited state was quite high in energy to deal with C-H bond activation [30]. As shown in Fig. S13-S14, the whole reaction of $^{1}$Pd and $^{2}Pd^{+}$ with ethane performed on the ground state PESs in a spin-conserving manner. Therefore, we only discussed the reaction mechanism Pd and $Pd^{+}$ with ethane on the ground state PESs. The reaction was divided into the following three steps. Firstly, the first C-H bond of ethane was activated by $^{1}$Pd and $^{2}Pd^{+}$ with the energy barriers of 50 and 67 kJ/mol, respectively. Our calculation for the formation of $^{1}$IM2 was endothermic by 19 and 64 kJ/mol, respectively. For the second C-H bond activation in the $^{1}Pd/C_2H_6$ and $^{2}Pd^{+}/C_2H_6$, there was also competition between α-H and β-H similar to that in the reaction of $^{1}PdX^{+}$ with ethane. $^{1}$IM2 → $^{1}$IM3 was the process of β-C-H bond activation; the energy barrier heights (relative to $^{1}$IM2) were 122 and 71 kJ/mol, respectively. The exothermicities of the step were 52 and 135 kJ/mol for $^{1}$Pd and $^{2}Pd^{+}$, respectively. Finally, $H_2$ was liberated by overcoming the dissociation energies of 54 and 26 kJ/mol, respectively. The α-C-H bond was activated in $^{1}$IM2 → $^{1}$IM4; the C-H bond activation barriers were 293 and 126 kJ/mol, respectively. The step was exothermic by 118 and 53 kJ/mol, respectively. Subsequently, $H_2$ was liberated by overcoming the dissociation energies of 41 (for $^{1}$Pd) and 39 kJ/mol (for $^{2}Pd^{+}$), respectively. Compared with β-C-H bond activation, the α-C-H bond activation has less competition ability in the reaction of $^{1}$Pd and $^{2}Pd^{+}$ with ethane. We

**Table 3** The rate constants of rate-determining step at 298 K

| $T$ = 298 K | $^{1}Pd(C_2H_5)^{+}$ + HX ($s^{-1}$) | $^{1}PdH(C_2H_4)^{+}$ + HX ($s^{-1}$) | $^{1}PdX(C_2H_4)^{+}$ + $H_2$ ($s^{-1}$) |
|---|---|---|---|
| $^{1}PdF^{+}$ | $2.04 \times 10^{7}$ | $3.12 \times 10^{6}$ | $4.5 \times 10^{-27}$ |
| $^{1}PdCl^{+}$ | $1.81 \times 10^{4}$ | $2.61 \times 10^{4}$ | $1.42 \times 10^{-10}$ |
| $^{1}PdBr^{+}$ | $0.5 \times 10^{2}$ | $2.09 \times 10^{2}$ | $1.87 \times 10^{-7}$ |
| $^{1}PdH^{+}$ | $1.26 \times 10^{2}$ | $9.49 \times 10^{2}$ | |
| $^{1}PdCH_3^{+}$ | $4.94 \times 10^{7}$ | $2.32 \times 10^{8}$ | |

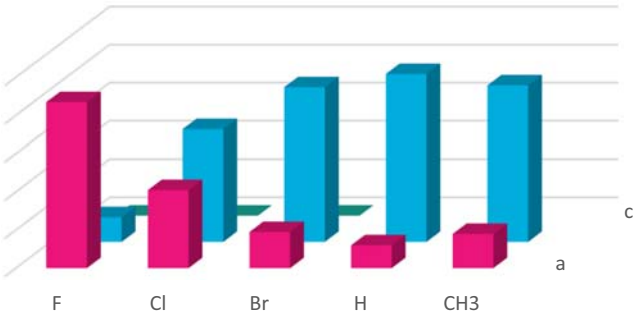


**Fig. 13** Branching ratios for product (**a**) $^{1}Pd(C_2H_5)^+ + HX$(■), (**b**) $^{1}PdH(C_2H_4)^+ + HX$ (■), and (**c**) $^{1}PdX(C_2H_4)^+ + H_2$ (■)

concluded that the main reaction path was $1^{1}IM1 \rightarrow {}^{1}TS1/2 \rightarrow {}^{1}IM2 \rightarrow {}^{1}TS2/3 \rightarrow {}^{1}IM3$ in the reaction of $^{1}Pd$ and $^{2}Pd^+$ with ethane. The highest energy relative to the ground state reactants was 123 and 33 kJ/mol in the whole $^{1}Pd$ and $^{2}Pd^+$ with ethane reaction. Comparing the reactivity of atomic Pd and $Pd^+$ with ethane, the highest energy in $^{1}Pd/C_2H_6$ was 90 kJ/mol higher than that of $^{2}Pd^+/C_2H_6$. It was indicated that the $^{2}Pd^+$ was easier to activate the C-H of $C_2H_6$ than the neutral atomic Pd.

Despite the qualitative similarities among the reaction paths, there were significant differences in some aspects. NBO calculations showed that the ground states $^{1}Pd$ and $^{2}Pd^+$ had a valence electron population of $4d^{10}$ and $4d^{9}$ on Pd atom, respectively. Compared with atomic $^{1}Pd$, the population of the 4d orbitals of Pd in cations $^{2}Pd^+$ and $^{1}PdX^+$ was unfilled. For $PdF^+$, $PdCl^+$, and $PdBr^+$, the high spin states were the ground states, while the ground states were the low spin states in Pd, $Pd^+$, $PdH^+$, and $PdCH_3^+$. In the ground states of $PdF^+$, $PdCl^+$, and $PdBr^+$, the valence electron population of the 4d orbitals of Pd from F to Br gradually increased; similarly from $Pd^+$ to $PdH^+$, $PdCH_3^+$, and atomic Pd, the valence electron population of the 4d orbitals on Pd also increased in the ground states of $Pd^+$ to $PdH^+$, $PdCH_3^+$, and atomic Pd. The reaction of $PdX^+$ (X = F, Cl and Br) with ethane started from triplet state and then through CPs point; the final proceeded in the singlet state PESs. This reaction was typical "two-state reaction." In contrast, for $^{1}Pd$, $^{2}Pd^+$, and $PdX^+$ (X = H and $CH_3$) with $C_2H_6$, the overall reaction was performed on the ground state PESs in a spin-conserving manner. In $^{1}PdX^+/C_2H_6$ (X = F, Cl, and $CH_3$), the first hydrogen atom H1 was transferred through the OA/RE reaction mechanism, whereas for $^{1}PdX^+/C_2H_6$ (X =H and Br), H1 was transferred via the σ-CAM mechanism. Before intermediate $^{1}IM3$, the reaction mechanism of $^{1}Pd$, $^{2}Pd^+$, and $^{1}PdX^+$ ethane was very similar. In reaction of $PdX^+$ (X = F, Cl, and Br) with $C_2H_6$, the hydrogen atom H1 back transfer combined with H2 or H4 on Pd to afford $H_2$, whereas those of $PdH^+$ and $PdCH_3^+$ were not observed. In the reaction of $^{1}PdX^+$ with ethane, the activation of the first C-H bond was exothermic, and the second C-H bond was

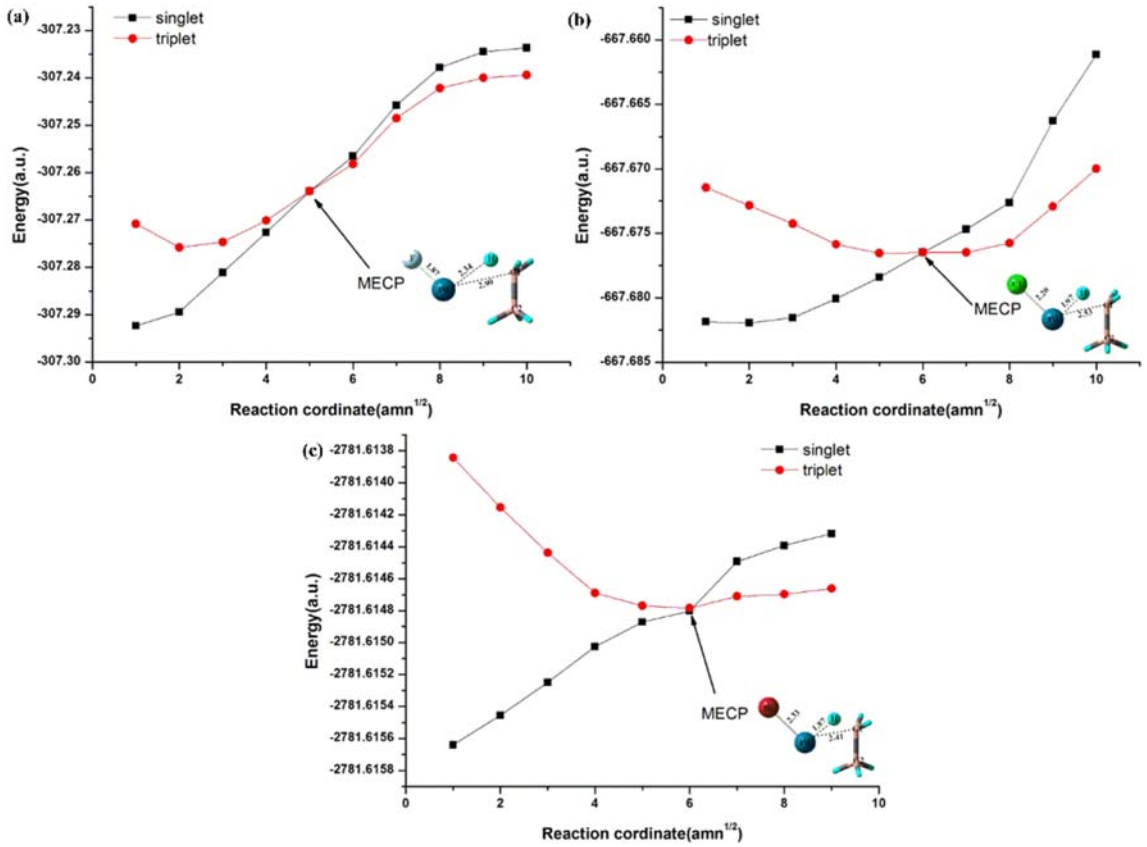


**Fig. 14** Potential energy curve-crossing diagrams. **a** $PdF^+$. **b** $PdCl^+$. **c** $PdBr^+$

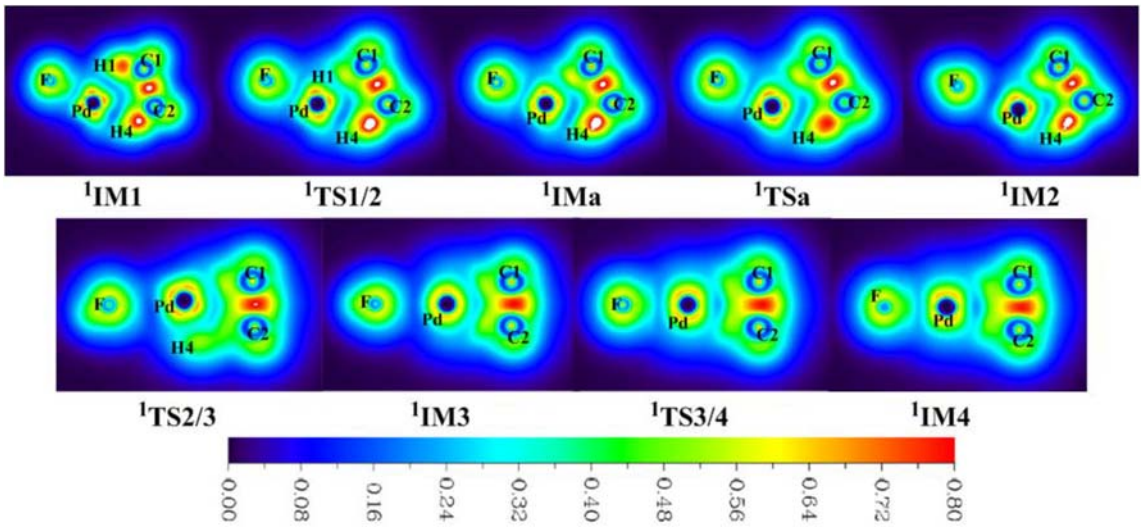


**Fig. 15** Localized orbital locator (LOL) map of stationary points on the main path

endothermic, whereas for $^1$Pd and $^2$Pd$^+$, the first C-H bond activation was endothermic and the second C-H bond activation was exothermic. For PdX$^+$/$C_2H_6$ (X = F, Cl, and Br), the main products were HX with a small amount of $H_2$. In the reaction of Pd, Pd$^+$, and PdH$^+$ with $C_2H_6$, only $H_2$ was liberated. For PdCH$_3^+$, only $CH_4$ was produced. Dehydrogenation was the rate-determining step of reaction $^1$PdX$^+$/$C_2H_6$ (X = F, Cl, and Br), the rate constants gradually increased from F to Br. In $^1$Pd, $^2$Pd$^+$, and $^1$PdH$^+$, the activation of the second C-H bond was the rate-determining step. From $^1$Pd to $^2$Pd$^+$ and $^1$PdH$^+$, the rate constants also gradually increased (rate constants were $1.08 \times 10^{-9}$ for $^1$Pd and 0.45 for $^2$Pd$^+$). The rate-determining step was the release of $CH_4$ molecule at the PdCH$_3^+$/$C_2H_6$ system. Based on the above data, the order of reactivity of atomic Pd-, Pd$^+$-, and PdX$^+$-activated C-H bond of ethane has been listed as PdH$^+$ > PdF$^+$ > PdCH$_3^+$ >PdCl$^+$ > PdBr$^+$ > PdCH$_3^+$ > Pd$^+$ >Pd.

The above mentioned was the activation process of C-H bond in all systems, while the activation of C-C bond was only observed in the $^1$Pd/$C_2H_6$ system, as shown in Fig. S15. In the activation of the C-C bond process, it was observed that no methane was formed while formation the complex $CH_3$-Pd-$CH_3$. The barrier height of the TS in C-C bond activation was 26 kJ/mol lower than that of C-H bond. It is indicated that the reaction efficiency of atomic Pd activation C-H bond of ethane was lower than that of activated C-C.

## Conclusions

The reaction mechanism of PdX$^+$ activation C-H bond of $C_2H_6$ was investigated by B3LYP method under DFT theory. The front molecular orbital of the initial complexes was analyzed by density of states (DOS). The d orbital of palladium and the p or s orbital of ligand had significant contribution to the HOMO orbits. The first hydrogen atom can be transferred in two different ways, OA/RE (for F, Cl and $CH_3$) and σ-CAM (for Br and H). During the second hydrogen transfer, the cations PdX$^+$ exhibited high bond selectivity for the activation of α-C-H and β-C-H bonds in ethane. In the second hydrogen transfer process, the α-hydrogen transfer process had less competitive abilities than that of β-hydrogen. CPs between the two PESs could be observed and effectively decreased the activation barrier in PdX$^+$ (X = F, Cl, and Br). The most favorable reaction pathway started from triplet PESs and then proceeded through the singlet PESs to liberate HX and $H_2$. In PdX$^+$ (X = H and $CH_3$) system, the whole reaction proceeded on the ground state PESs in a spin-conserving manner. Theoretical studies on the reactions PdX$^+$ (X = F, Cl, and Br) with ethane had showed that the loss of HX was more facile than dehydrogenation. The final main products of the reaction of PdX$^+$ (X = F, Cl, and Br) with ethane were HX and small amount of $H_2$. In the reaction of PdH$^+$ with $C_2H_6$, only $H_2$ was liberated. For PdCH$_3^+$, only $CH_4$ was produced. Adding appropriate ligands could enhance the catalytic efficiency of palladium; the order of reactivity of atomic Pd-, Pd$^+$-, and PdX$^+$-activated C-H bond of ethane has been listed as PdH$^+$ > PdF$^+$ > PdCH$_3^+$ >PdCl$^+$ > PdBr$^+$ > PdCH$_3^+$.

## References

1. Labinger JA, Bercaw JE (2002) Understanding and exploiting C-H bond activation. Nature 417:507–514
2. Enger BC, Lødeng R, Holmen A (2008) A review of catalytic partial oxidation of methane to synthesis gas with emphasis on reaction mechanisms over transition metal catalysts. Appl Catal A Gen 346:1–27
3. Roithová J, Schröder D (2010) Selective activation of alkanes by gas-phase metal ions† - Chemical Reviews (ACS Publications). Chem Rev 110:1170–1211

4. Zhu B, Guan W, Yan LK, Su ZM (2016) Two-state reactivity mechanism of benzene C-C activation by trinuclear titanium hydride. J Am Chem Soc 138:11069–11072
5. Sicilia E, Russo N (2002) Theoretical study of ammonia and metactivation by first-row transition metal cations $M^+$ (M = Ti, V, Cr). J Am Chem Soc 124:1471–1480
6. Blomberg MRA, Siegbahn PEM (1994) Svensson M, Reaction of second-row transition-metal cations with methane. J Phys Chem 98:2062–2071
7. Holthausen MC, Fiedler A, Schwarz H, Koch W (1996) How does $Fe^+$ activate C-C and C-H bonds in ethane? A theoretical investigation using density functional theory. J Phys Chem 100:6236–6242
8. Mandich ML, Steigerwald ML, Reents WD (1986) The effects of chloro substitution on the electronic structure of $ClCr^+$, $ClMn^+$, and $ClFe^+$ and their reactivity with small alkanes. J Am Chem Soc 108:6197–6202
9. Roithová J, Schröder D (2010) Selective activation of alkanes by gas-phase metal ions. Chem Rev 110:1170–1211
10. Schlangen M, Schrçder D, Schwarz H (2007) Ligand and substrate effects in gas-phase reactions of $NiX^+$/RH couples (X = F, Cl, Br, I; R = $CH_3$, $C_2H_5$, $nC_3H_7$, $nC_4H_9$). Chem Eur J 13:6810–6816
11. Schlangen M, Schwarz H (2011) Probing elementary steps of nickel-mediated bond activation in gas-phase reactions: ligand- and cluster-size effects. J Catal 284:126–137
12. Shang R, Ilies L, Nakamura E (2017) Iron-catalyzed C-H bond activation. Chem Rev 117:9086–9139
13. Irikura KK, Beauchamp JL (1991) Electronic structure considerations for methane activation by third-row transition-metal ions. J Phys Chem 95:8344–8351
14. Schlangen M, Schwarz H (2007) Thermal activation of methane by group 10 metal hydrides $MH^+$: the same and not the same. Angew Chem Int Ed 46:5614–5617
15. Li WQ, Geng ZY, Wang YC et al (2009) Density functional theory studies of thermal activation of methane by $MH^+$ (M = Ru, Rh, and Pd). J Phys Chem A 113:1807–1812
16. Liu HQ, Geng ZY, Wang YC et al (2011) Theoretical investigation of thermal activation of methane by $[Pd(H)(OH)]^+$. Comput Theor Chem 963:470–474
17. Becke AD (1993) Density-functional thermochemistry. III. The role of exact exchange. J Chem Phys 98:5648–5652
18. Becke AD (1988) Density-functional exchange-energy approximation with correct asymptotic behavior. Phys Rev A 38:3098–3100
19. Lee C, Yang W, Parr RG (1988) Development of the Colle-Salvetti correlation-energy formula into a functional of the electron density. Phys Rev B 37:785–789
20. Gonzalez C, Schlegel HB (1990) Reaction path following in mass-weighted internal coordinates. J Phys Chem 94:5523–5527
21. Krishnan R, Binkley JS, Seeger R, Pople JA (1980) Self-consistent molecular orbital methods. XX. A basis set for correlated wave functions. J Chem Phys 72:650–654
22. Andrae D, Dolg M et al (1990) Energy-adjustedab initio pseudopotentials for the second and third row transition elements. Chim Acta 77:123–141
23. Reed AE, Curtiss LA, Weinhold F (1988) Intermolecular interactions from a natural bond orbital, donor-acceptor viewpoint. Chem Rev 88:899–926
24. Lu T, Chen F (2012) Multiwfn: a multifunctional wavefunction analyzer. J Comput Chem 33:580–592
25. Lu T, Chen F (2012) Quantitative analysis of molecular surface based on improved Marching Tetrahedra algorithm. J Mol Graph Model 38:314–323
26. Harvey JN, Aschi M, Schwarz H, Koch W (1998) The singlet and triplet states of phenyl cation. A hybrid approach for locating minimum energy crossing points between non-interacting potential energy surfaces. Theor Chem Accounts 99:95–99
27. Schmider HL, Becke AD (2000) Chemical content of the kinetic energy density. J Mol Struct THEOCHEM 527:51–61
28. Bader RFW (1990) Atoms in molecules: a quantum theory. Oxford University Press, Oxford
29. Frisch MJ, Trucks GW, Schlegel HB, Scuseria GE, Robb MA, Cheeseman JR, Scalmani G, Barone V, Mennucci B, Petersson GA, Nakatsuji H, Caricato M, Li X, Hratchian HP, Izmaylov AF, Bloino J, Zheng G, Sonnenberg JL, Hada M, Ehara M, Toyota K, Fukuda R, Hasegawa J, IshidaM NT, Honda Y, Kitao O, Nakai H, Vreven T, Montgomery Jr JA, Peralta JE, Ogliaro F, Bearpark MJ, Heyd J, Brothers EN, Kudin KN, Staroverov VN, Kobayashi R, Normand J, Raghavachari K, Rendell AP, Burant JC, Iyengar SS, Tomasi J, Cossi M, Rega N, Millam NJ, Klene M, Knox JE, Cross JB, Bakken V, Adamo C, Jaramillo J, Gomperts R, Stratmann RE, Yazyev O, Austin AJ, Cammi R, Pomelli C, Ochterski JW, Martin RL, Morokuma K, Zakrzewski VG, Voth GA, Salvador P, Dannenberg JJ, Dapprich S, Daniels AD, Farkas Ö, Foresman JB, Ortiz JV, Cioslowski J, Fox DJ (2009) Gaussian 09. Gaussian, Inc., Wallingford
30. Liu SL, Geng ZY, Wang YC et al (2012) Methane activation by $MH^+$ ( M = Os , Ir , and Pt ) and comparisons to the congeners of $MH^+$ ( M = Fe , Co , Ni and Ru , Rh , Pd ). J Phys Chem A 116:4560–4568
31. Malechi JG (2010) Synthesis, crystal, molecular and electronic structures of thiocyanate ruthenium complexes with pyridine and its derivatives as ligands. Polyhedron 29:1973–1979
32. Eyring H (1935) The activated complex in chemical reactions. J Chem Phys 3:107–115
33. DePuy CH (2002) Understanding organic gas-phase anion molecule reactions. J Organomet Chem 67:2393–2401
34. Mai BK, Kim Y (2015) The kinetic isotope effect as a probe of spin crossover in the C-H activation of methane by the $FeO^+$ cation. Angew Chem Int Ed Engl 54:3946–3951
35. Savin A et al (1992) Electron localization in solid-state structures of the elements: the diamond structure. Angew Chem Int Ed Eng 31:187–188
36. Jacobsen H (2008) Localized-orbital locator (LOL) profiles of chemical bonding. Can J Chem 86:695–702
37. Li P, Niu WX, Gao T, Wang HY (2014) Gas-phase water activation by Th atom: reaction mechanisms and topological analysis. Int J Quantum Chem 114:760–768